PAPER

Check for updates

Synthesis of micro–mesoporous ZSM-5 zeolite with microcrystalline cellulose as co-template and catalytic cracking of polyolefin plastics

Hongchang Yu,[a] Fuwei Li,[a] Wen He,[a] Caifeng Song,[a] Yansong Zhang,[a] Zhixia Li [ID] *[a] and Hongfei Lin[b]

Micro–mesoporous ZSM-5 with different Si/Al ratios (MZ-X, X = 27, 80, 150) were synthesized by adding microcrystalline cellulose (MCC) as co-template into the hydrothermal synthesis process of zeolites. The resultant ZSM-5 were used for catalytic cracking of high density polyethylene (HPDE) and polypropylene. It was found that introduction of MCC significantly enhanced the formation of mesopores and strong acid sites. MZ-27 achieved the highest oil yield: 21.5% for HPDE and 32.1% for polypropylene, and the light aromatics (BTEX) selectivity therein were 87.6% and 79.7%, respectively. HZ-150 (MCC-free ZSM-5, Si/Al = 150) achieved the highest gas yield: 85.4% for HDPE and 76.7% for polypropylene, and the light olefins ($C_{2-4}^{=}$) selectivity therein were 44% and 48.3%, respectively. The dense acidic sites and mesoporous structure of MZ-27 were responsible for its better activity for producing aromatic products. The moderate acidity and microporous structure of HZ-150 were helpful for producing light olefins from catalytic cracking of polyolefin plastics.

1. Introduction

Light olefins such as ethylene and propylene, and light aromatics such as benzene, toluene, ethylbenzene and xylene (BTEX), are important raw materials for numerous chemical industrial processes.[1] Currently, commercial production of light olefins and aromatics mainly depends on petroleum-based routes: the former involves steam cracking of naphtha and light diesel, and the latter mainly utilizes naphtha catalytic reformate. Along with the oil resource's gradual depletion, comes the huge challenge of developing non-petroleum routes for production of these fundamental raw materials.

Polyolefin plastics are extensively used in industrial production and daily life. Global production of resins and fibers increased from 2 Mt in 1950 to 380 Mt in 2015, a compound annual growth rate of 8.4% was reported during that period.[2] Meanwhile, the discharge of waste plastics has caused serious environmental problem and waste of the resources.[3–6] The main treatment solutions of waste plastics are landfills, incineration, mechanical recycling and thermal degradation.[7,8] Among them, thermal degradation is the most promising technology from resource recycling point of view.[9] Several papers reviewed research results on thermal and catalytic pyrolysis of plastics.[10–12] The thermal pyrolysis was generally carried out at high temperature, and achieved a wide product distribution including gases, liquid oils, waxes and solid residue. The catalytic pyrolysis could convert plastics into valuable products e.g. waxes, BTX and light olefins with high selectivity at lower temperature and reaction time. Product selectivity strongly depended on the natures of catalysts (porosity and acidity). A microporous catalyst with high acidity e.g. HZSM-5 produced more gases, while macroporous catalysts with less acidity e.g. MCM-41 enhanced the formation of liquid oils. The spent FCC catalyst was used for the cracking of plastics because of its cheapness and high activity, which obtained a high liquid yield, mainly including gasoline fractions.[11]

In order to minimize heat transfer limitations and physical problems (sticky nature) in the pyrolysis of plastics, different reactors have been proposed, e.g. fixed bed, fluidized bed, spouted bed and screw kiln.[10] The benefits for the tubular fixed bed reactors is that the gas residence time in these reactors could be regulated by adjusting the flow rate of carrier gas. Fluidized bed reactors are characterized by their high heat and mass transfer rates. However, bed defluidization due to agglomeration of particles coated with fussed plastic would occur under severe operating conditions. Spouted beds are an alternative to fluidized beds, and are characterized by its vigorous gas–solid contact. Accordingly, bed defluidization could be avoided. Besides, screw kilns were used for pyrolysis of plastics, which make polymer pyrolysis handy and smooth. The plastics alone or the mixture of plastics with catalysts was feed into reactor, and polymer residence time was controlled by varying the rotation speed of the screw.

[a]School of Chemistry and Chemical Engineering, Guangxi University, Nanning 530004, China. E-mail: zhixiali@hotmail.com

[b]Guangxi Bossco Environmental Protection Technology Co., Ltd., Nanning 530007, China

In situ catalytic cracking is the primary way for all kinds of reactors. However, it has to face two main drawbacks: impurities in waste plastics would cause inactivation of catalysts, and there is serious diffusional restriction for bulky polymeric molecules accessing the active sites inside the porous catalysts. In order to improve the efficiency of the catalytic step, *ex situ* catalytic cracking technology was developed. *Ex situ* cracking can be arranged by a fixed bed reactor (or fluid bed/spouted bed reactor) connected in-line with a tubular reactor, with the aim of the first reactor being pyrolysis to yield oil and waxes. In the second reactor, the volatiles formed in the first reactor are subsequently pyrolyzed at high temperatures and short residence times. A high gases yield is easily obtained by *ex situ* cracking. Another advantage by *ex situ* cracking is that two steps (pyrolysis and catalytic cracking) can be operated under different conditions.[10]

So far, a lot of researches have been carried out on catalytic cracking of waste plastics for production of chemicals. For instance, plastic film wastes were cracked over nanocrystalline HZSM-5 zeolite for selective production of light olefins.[9] Pyrolysis-catalysis of high density polyethylene (HPDE) was carried out in a fixed bed, two stage reactor for the production of aromatics, and found that loading of 1 wt% Ga, Fe or Ru on the Y-zeolite catalysts led to a higher production of aromatic hydrocarbons in the product oil (aromatic content >90%).[13] Nishino *et al.*[14] used a Ga-ZSM-5 catalyst for the catalytic pyrolysis of industrial plastic waste, a liquid product yield >50% consisting of >80% aromatic compounds were obtained. These results indicate that the zeolites especially HZSM-5, are the most effective catalyst for catalytic conversion of waste plastics into aromatics. Aguado *et al.*[15] studied the catalytic cracking of PP over HMCM-41, SiO_2–Al_2O_3 and HZSM-5, and reported 99.2% conversion for HMCM-41 and only 11.3% for HZSM-5. The higher activities of HMCM-41 was deemed to be associated with the presence of highly accessible acid sites in the mesoporous catalysts. A mesoporous structure of catalysts would be helpful for the catalytic cracking of bulky polymers.

Cellulose is a chain macromolecule, and represents one kind of major renewable and cheap resource. In this work, three micro–mesoporous ZSM-5 with different Si/Al ratio (27, 80, 150) were hydrothermally synthesized using tetrapropyl ammonium bromide as main template, and microcrystalline cellulose (MCC) as co-template, with the aim of reducing the production cost of mesoporous catalysts which are often produced by using expensive organic structure directing agents.[16–18] The effect of MCC addition on acidity and pore structure of zeolites were investigated. The obtained ZSM-5 were used for catalytic cracking of HDPE and PP to produce high added-value chemicals *e.g.* light olefins and BTEX.

2. Experimental

2.1 Materials

Colloidal silica (Ludox, 40%, Guangzhou Suize Co. Ltd), ammonium chloride (NH_4Cl, 99.5%, Sinopharm Chemical Reagent Co. Ltd), sodium aluminate ($NaAlO_2$, Al_2O_3 wt% = 50 Sinopharm), sodium hydroxide (NaOH, 96%, Aladdin

Reagents), tetrapropyl ammonium bromide (TPABr, 98%, Aladdin), microcrystalline cellulose (MCC, Beijing Solarbio Science & Technology Co. Ltd), and sulfuric acid (H_2SO_4, 98%) were used as received. PP (d = 910 kg m^{-3}) and HDPE (d = 951 kg m^{-3}) were cylindrical pellets with particle size about 4 mm, provided by China National Petroleum Corporation.

2.2 Synthesis of the catalysts

ZSM-5 samples with different Si/Al ratio (27, 80, 150) were synthesized according to a hydrothermal method.[19,20] 0.8 g MCC was soaked in 10 g H_2O for 24 h to obtain the MCC suspension, denoted as MCS. The molar compositions of three ZSM-5 precursors was $200SiO_2$–xAl_2O_3–$35NaOH$–$10TPABr$–$15H_2SO_4$–$2445H_2O$. Precursors A, B and C were obtained by setting x at 7.4, 2.5 and 1.33, respectively. A typical synthesis process was as follows: first, a certain amount of NaOH and $NaAlO_2$ were dissolved in H_2O to form solution I. A certain amount of Ludox and template were dispersed in H_2O to form solution II. Solution I was added into solution II drop by drop with agitation to form gel mixture. A certain amount of moderate concentrated H_2SO_4 was added to the mixture to adjust gel pH to 9 to obtain the precursors. Then, MCS was added into the precursor gel, and continuously stirred for 4 h. Finally, the resultant gel was transferred into a stainless-steel Teflon-lined autoclave and crystallized at 180 °C for 48 h. The obtained solid product was filtered, washed with distilled water until the pH of the filtrate was 7, and then dried at 105 °C overnight. The resultant product was afterwards calcined at 550 °C for 6 h to remove the organic templates. The obtained sample was defined as NaZSM-5 zeolite. HZSM-5 zeolite was obtained by ion-exchanging NaZSM-5 zeolite two times with 1 mol L^{-1} NH_4Cl solution (liquid/solid = 10 mL g^{-1}) at 80 °C for 4 h. The solid sample was filtered, dried at 105 °C overnight, and calcined at 550 °C for 6 h. The obtained HZSM-5 was tableted, granulated and sieved to obtain 20–30 mesh catalyst. The three catalyst samples derived from three precursors A, B and C were correspondingly denoted as MZ-*X* (*X* = 27, 80, 150) according to the different Si/Al ratio. As reference, the MCC-free zeolites (denoted as HZ-*X*, *X* = 27, 80, 150) were synthesized according to the above procedure but no addition of MCS.

2.3 Characterizations of catalysts

The crystalline structure of samples was determined by X-ray powder diffraction (XRD) using a Rigaku SmartLab3 instrument in the range of 5–50 °C at a scanning rate of 8° min^{-1}. The surface morphology of the catalysts was observed on Hitachi SU8220 scanning electron microscopy (SEM). N_2 adsorption–desorption isotherm was performed at −196 °C, employing the Quantachrome NOVA 2200e instruments. The pore size distribution was obtained using the non-local density functional theory (NLDFT) model.

The ammonia temperature-programmed desorption (NH_3-TPD) was carried out by AutoChemII2920 to characterize the acidity of the catalysts. Prior to adsorption experiments, 300 mg of catalyst was pretreated at 200 °C for 1 h in a He flow. Upon cooling to 50 °C, the samples were saturated with a NH_3 flow for

1 h, and then the physically absorbed NH_3 was removed through purging with He gas for 1 h. The samples were then heated to 800 °C at a heating rate of 10 °C min^{-1} in He flow. Desorbed ammonia was recorded by a thermal conductivity detector (TCD). The total acidity amount was calculated from the peak area compared to a standard peak area of 1 mL of NH_3 based on NH_3-TPD curve. The distribution of weak acid, medium acid, and strong acid was calculated from the peak area from Gaussian fitting of the NH_3-TPD profiles.

Infrared spectroscopic (IR) analysis was carried out on a Shimadzu spectrometer (IRTracer-100) with scanning range from 4000 cm^{-1} to 400 cm^{-1} using the KBr pellet method. The thermal stability of coke was analysed by a thermogravimetric analyzer (TGA, 209F3, Tarsus) in a 30 : 70 (v/v) O_2/N_2 mixture.

2.4 Catalytic performance tests

HDPE and PP were dried at 80 °C for 2 h before use. The catalytic cracking experiments were performed in a fixed-bed quartz tube reactor. For each run, the catalyst (0.5 g) was loaded into reactor, and heated to 550 °C in N_2 stream (the flow rate: 40 mL min^{-1}). The plastic sample (1.0 g) was fed in the reactor in three equal installments at a 5 min interval, and reacted for another 11 min. After flowing out from the reactor, the products were cooled at about −10 °C. The obtained gas was collected with a gas collecting bag, and its volume was recorded. Liquid products were weighed and analysed.

2.5 Product analysis

The gas products were analysed using gas chromatography (GC, FULI-9790II, China) equipped with a flame ionization detector (FID) and a capillary column of HP-PLOT/Q. The following temperature program was used: hold at 25 °C for 4 min, heated to 240 °C at 15 °C min^{-1}, and hold at 240 °C for 15 min. The qualitative and quantitative analyses were performed using the standard gases.

The liquid products were analysed by GC-MS (GC7820A, MS 5977E, Agilent) equipped with a HP-5MS fused silica capillary column (30 m × 250 μm × 0.25 μm). The GC had been calibrated by typical polymer pyrolytic oil components using standard chemicals such as benzene, toluene, p-xylene and m-xylene. The oven temperature program was set as follows: hold at 60 °C for 5 min, heated to 290 °C at 10 °C min^{-1}, and hold at this temperature for 5 min; the injector and interface temperature were maintained at 290 °C.

The total gas production (TGP), the liquid yield (Y_L), the coke yield (Y_C), the gas yield (Y_G), the selectivity to the light olefin (S_{LO}), the selectivity to BTEX aromatics (S_{BTEX}), were calculated by the following equations, respectively:

$$TGP \ (mL \ g^{-1}) = V_{TGP}/M_0 \times 100\% \tag{1}$$

$$Y_L \ (\%) = M_1/M_0 \times 100\% \tag{2}$$

$$Y_C \ (\%) = (M_{c0} - M_{c1})/M_0 \times 100\% \tag{3}$$

$$Y_G \ (\%) = 1 - Y_L - Y_C \tag{4}$$

$$S_{LO} \ (\%) = x(C_2H_4) + x(C_3H_6) + x(C_4H_8) \tag{5}$$

$$\begin{aligned} S_{BTEX} \ (\%) = {} & y(benzene) + y(toluene) + y(ethylbenzene) \\ & + y(xylene) \end{aligned} \tag{6}$$

where V_{TGP} is the total volume of gas product excluding N_2 (mL), M_0 is the mass of the feedstock, M_1 is the mass of liquid product (g). M_{c0} is the mass of the spent catalysts before calcination (g), and M_{c1} is the mass of the spent catalyst after calcination at 550 °C (g). x is the molar percentage content of light olefins in the gas product (%), y is the relative quality percentage of BTEX aromatics in the liquid product (%). The data of TGP, Y_L, Y_G, Y_C, S_{LO} and S_{BTEX} are the average value of three parallel experiments.

2.6 Stability experiments of catalysts

The stability of the catalysts was determined by continuous catalytic cracking of HDPE and PP over MZ-27 at 550 °C in N_2 stream for 600 min. For each test, 0.3 g plastic sample was fed in the reactor every 5 min until the end of reaction. Liquid products were collected for 1 min every 30 min. Liquid yield and BTEX selectivity were analysed.

3. Result and discussion

3.1 Characterization of the catalysts

The XRD patterns of all samples are shown in Fig. 1. The XRD were similar, and consisted of sharp peaks near 8°, 8.8°, 23.1° and 23.3°, matched well with the characteristic peaks of ZSM-5.[21] Lattice parameters of catalysts were calculated and depicted in Table 1. The lattice constants were close to the value of ZSM-5 reported in a previous study.[22] The relative crystallinity (calculated based on the sum of peak area between 22.5–25° in XRD pattern of the ZSM-5 samples compared to that of HZ-150) is 79.6% for HZ-27, 70.1% for MZ-27, 99.2% for HZ-80, 72.5% for MZ-80 and 90.2% for MZ-150. The crystallinity of MCC-adding catalysts decreased compared to the MCC-free catalysts. MCC could depolymerize to cellulose monomers, and even degrade to other micromolecules like monosaccharide and carboxylic acids during the process of gel crystallization.[23,24] These degraded components could hinder crystallization reaction of silica species and aluminium species, consequently leading to the decrease in the crystallinity of MZ-X catalysts. The pH value of the reaction solution after crystallization reduced to 8 (initial pH was 9), indicating that hydrolysis reaction of MCC occurred and produced acidic compounds.[25]

Fig. 2 shows the IR spectra of all samples. There was strong bands at 796 cm^{-1}, which is owing to the corresponding T–O–T symmetric stretching mode, 546 cm^{-1} resulted from the framework vibration at pentacyl ring which is characteristic of the MFI-type zeolite structure, and 450 cm^{-1} caused from vibration of the T–O–T bending bond, where T is Si or Al atoms.[26] These results indicated that all samples contained ZSM-5 structure.

The N_2 adsorption–desorption isotherms and the pore size distribution of samples are illustrated in Fig. 3. As can be seen in Fig. 3(a), HZ-27, MZ-27 and MZ-80 showed an approximately
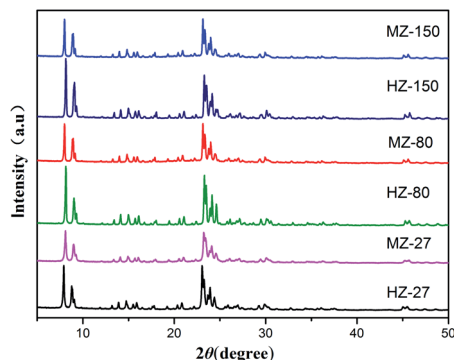
Fig. 1   XRD patterns of the HZ-*X* and MZ-*X* samples.

Table 1   Lattice parameters of the prepared ZSM-5 samples

Catalysts	Relative crystallinity (%)	Lattice constants (nm)			V_{cell} (nm^3)
		a	b	c	
HZ-27	79.6	1.9992	1.9919	1.3347	5.315
MZ-27	70.1	2.0102	1.9897	1.3413	5.365
HZ-80	99.2	2.0088	1.9802	1.3386	5.325
MZ-80	72.5	2.0133	1.9828	1.3326	5.320
HZ-150	100	1.9987	1.9902	1.3401	5.331
MZ-150	90.2	2.0087	1.9815	1.3371	5.322

IV-type isotherm with a hysteresis loop at a high relative pressure ($P/P_0 = 0.4$–0.9), indicating the presence of mesopores. As shown in Fig. 3(b), the major pore diameter of all samples was around 3 nm. More large pores with diameter 3–14 nm were present in MZ-27 and MZ-80. All samples had a high specific surface area (>370 m^2 g^{-1}) and an average pore diameter about 3–4 nm (Table 2). The S_{ext} and V_{meso} of MZ-*X* samples were obviously larger than the corresponding HZ-*X* samples with the same Si/Al ratio. These results indicated that introduction of MCC into the hydrothermal synthesis process of zeolites significantly enhanced the formation of mesopores. The presence of mesopores in ZSM-5 is useful for accelerating the diffusion of bulkier molecules and accessing the active sites on catalysts.[27]
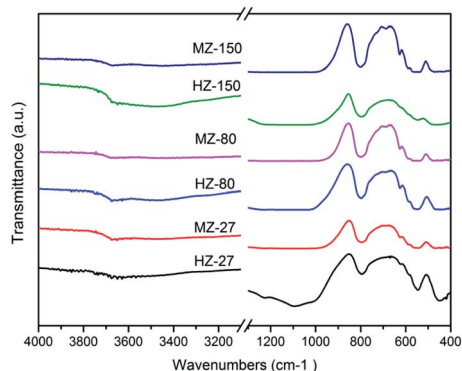
Fig. 2   IR spectra of the HZ-*X* and MZ-*X* catalysts.
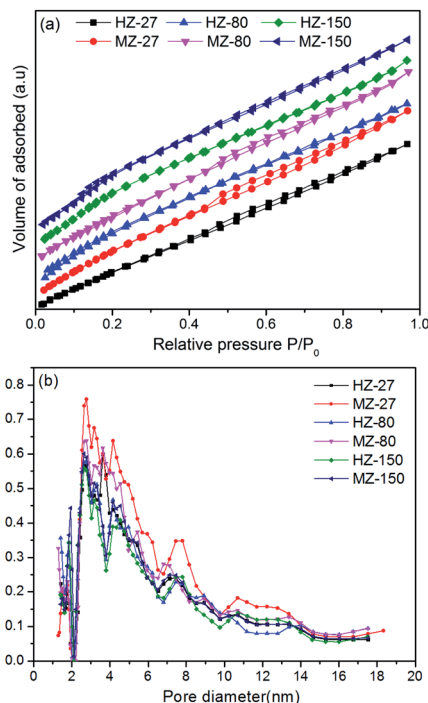
Fig. 3   N$_2$ adsorption–desorption isotherms (a) and pore size distributions (b) of HZ-*X* and MZ-*X* catalysts.

The acid amount and relative acid strength in ZSM-5 samples were determined by NH$_3$-TPD. The results are shown in Fig. 4 and Table 2. The weak acid, medium acid and strong acid were defined in the temperature region 100–230 °C, 230–350 °C, and 350–550 °C, respectively, in NH$_3$-TPD curves. It was found that peak area and total acid amount decreased with increasing Si/Al ratio. This was consistent with the findings reported in previous research.[28] The acid amount is related to the density of acidic sites, which are generated by Al species in the catalysts consisting of silica and alumina.[29] In addition, it can be seen in Table 2, more strong acid sites were formed in MCC-adding samples compared to the MCC-free samples with same Si/Al ratio. This could be due to MCC-derived degraded compounds inducing the formation of new Brønsted acid sites on catalysts during crystallization process.

SEM images of the prepared ZSM-5 samples is shown in Fig. 5. As can be seen, HZ-27 and MZ-27 existed as spherical particles, and were actually aggregates of small needle-like crystals. HZ-80, MZ-80, HZ-150 and MZ-150 showed a typical "coffin" morphology.[30] The difference would arise from the different crystallization reaction mechanisms. In the case of preparation of HZ-27 and MZ-27, zeolites was likely produced *via* a solid hydrogel transformation mechanism, and the high content of Na$^+$ in the gel (added with introduction of NaAlO$_2$) could play important structure directing role. The presence of Na$^+$ helped to form the primary aluminosilicate species of five-membered structures in the initial gel, and subsequently facilitate the condensation or rearrangement of the primary structure building units.[31,32] Compared with HZ-27, the particle size of the aggregates of MZ-27 were larger, and the needle-like

Table 2 Textural and acidic properties of different ZSM-5 zeolites

Catalyst	S_{BET} [a] ($m^2\,g^{-1}$)	S_{ext} [b] ($m^2\,g^{-1}$)	D_{aver} [c] (nm)	V_{total} [d] ($cm^3\,g^{-1}$)	V_{micro} [b] ($cm^3\,g^{-1}$)	V_{meso} [e] ($cm^3\,g^{-1}$)	Total acid ($cm^3\,g^{-1}$)	Percentage of acid sites in total acid (%) Weak acid	Medium acid	Strong acid
HZ-27	412.9	253.1	3.67	0.378	0.067	0.311	4.68	62.05	24.65	13.30
MZ-27	371.6	282.7	4.28	0.447	0.054	0.393	4.49	50.39	35.57	14.04
HZ-80	461.3	276.9	3.27	0.388	0.092	0.296	3.11	57.94	33.87	8.19
MZ-80	453.3	341.3	3.73	0.442	0.078	0.364	2.83	55.57	21.95	18.46
HZ-150	524.3	257.3	3.22	0.394	0.111	0.283	1.09	48.02	38.11	13.86
MZ-150	485.6	303.2	3.25	0.421	0.101	0.320	0.98	44.69	36.40	18.91

[a] S_{BET} (BET surface area) was obtained from the adsorption isotherm. [b] S_{ext} (external surface areas) and V_{micro} (micropore volumes) were calculated using t-plot method. [c] D_{aver} (average pore size) was obtained from average pore size. [d] V_{total} (total pore volumes) was obtained at the relative pressure $(P/P_0) = 0.99$. [e] $V_{meso} = V_{total} - V_{micro}$.
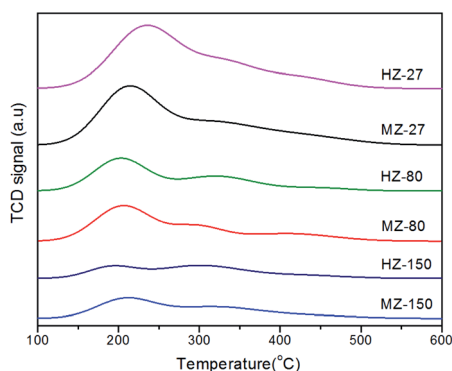
Fig. 4 NH$_3$-TPD profiles of the MZ-X and HZ-X samples.

crystals in the aggregates were obviously larger and more dispersive. This was probably ascribed to a synergistic structure directing effect of MCC. There is a lot of –OH groups on the surface of MCC, the considerable interaction between –OH and silicon and aluminum species (*e.g.* hydrogen bond) probably induces the growth of zeolite crystals in different direction; besides, the negative-charged degraded products from basic hydrolysis of MCC (*e.g.* glucose, straight-chain and branch-chain hydroxy-monocarboxylic and dicarboxylic acids) would produce steric effect,[25] and hamper the cross-linking reaction of silicon and aluminum species in horizontal direction, consequently producing one-way growing needle-like crystals. Therefore, we speculated that there will be a synergy effect between TPABr, Na$^+$ and MCC.

In the case of preparation of zeolites with higher Si/Al ratio *e.g.* HZ-80, MZ-80, HZ-150 and MZ-150, zeolites could be produced by following a solution-mediated transport mechanism. Owing to lack of Na$^+$ in gel, there were little primary structure building units of five-membered structures formed in the solid-phase of the gel, and the nucleation of gel should occur in the liquid phase.[31] The production of large ZSM-5
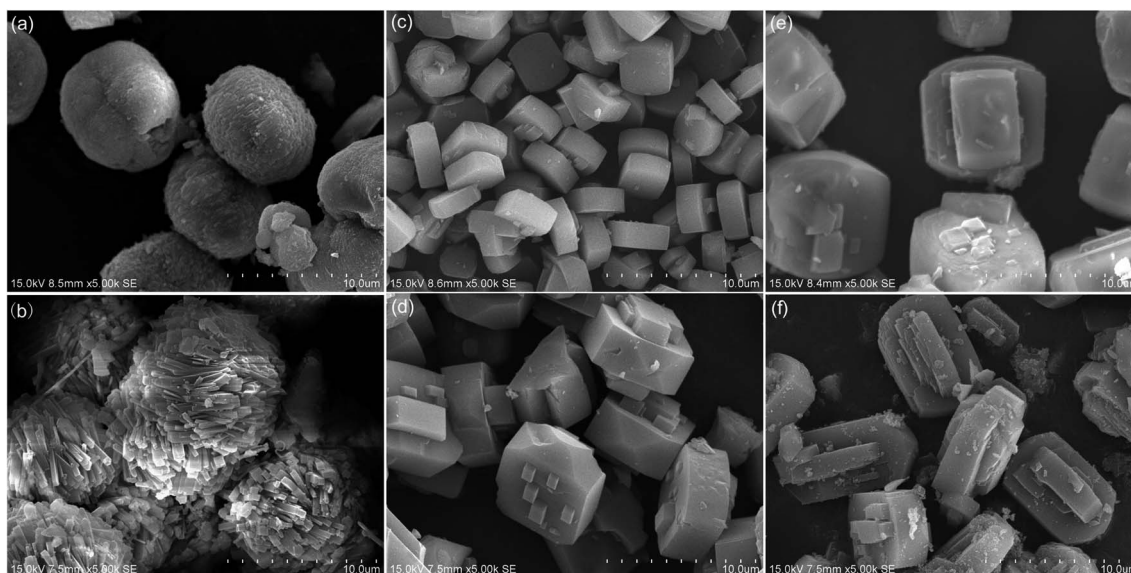

Fig. 5 SEM images of the prepared ZSM-5 samples: (a) HZ-27, (b) MZ-27, (c) HZ-80, (d) MZ-80, (e) HZ-150, (f) MZ-150.

Table 3 Product yield and product distribution from cracking of HDPE over the prepared catalysts

	Catalysts					
	HZ-27	MZ-27	HZ-80	MZ-80	HZ-150	MZ-150
Y_{TGP} (mL g^{-1})	433	402	446	432	468	444
Y_L (%)	20.8	21.5	17.5	18.8	13.9	14.3
Y_C (%)	1.6	1.2	1.2	0.8	0.7	0.5
Y_G (%)	77.6	77.3	81.3	80.4	85.4	85.2
Gas product (%)						
C_2H_4	13.8	13.5	13.1	12.9	13.9	14.1
C_3H_6	17.3	13.8	18.5	17.3	24.8	19.8
$n\text{-}C_4H_8$	5.5	4.0	5.3	6.1	5.3	8.9
CH_4	4.4	6.6	4.9	3.0	2.2	2.3
C_2H_6	2.9	3.7	1.3	2.9	1.6	2.4
C_3H_8	16.9	20.3	18.3	18.9	10.3	13.9
$n\text{-}C_4H_{10}$	4.7	4.6	4.9	5.8	6.7	5.2
$C_{2-4}^=$	36.6	31.3	36.9	36.3	44.0	42.8
C_{1-4}	28.9	35.2	29.4	30.6	20.8	23.8
Others	34.5	33.5	33.7	33.1	35.2	33.4
Liquid product (%)						
Benzene	5.9	8.7	4.9	6.4	4.5	4.6
Toluene	23.4	28.3	21.3	25.7	19.6	23.2
Ethylbenzene	7.3	5.7	5.3	6.5	6.3	6.7
Xylene	41.3	44.9	42.5	46.2	35.8	38.4
BTEX	77.9	87.6	74	84.5	66.2	72.9
Aliphatic hydrocarbons	7.8	1.8	8.1	3	19.2	16.9
Others	14.3	10.6	17.9	12.2	14.6	10.2

crystals indicated the lack of nuclei in the liquid phase of gel. The interaction between MCC and silicon and aluminum species could restrain the diffusion of silicon and aluminum species in the solid-phase of the gel into the liquid phase, and thus influence the formation of nuclei as well as growth of crystals, consequently leading to the formation of a larger particle of MZ-80 compared to HZ-80.

3.2 Catalyst performance

Catalytic cracking reactions of HDPE and PP were carried out at 550 °C in N_2 stream over all prepared ZSM-5 samples. Gas yield, liquid yield, and product distribution are summarized in Tables 3 and 4.

3.2.1 Catalytic cracking of HDPE. As shown in Table 3, the gas products including light olefins ($C_{2-4}^=$) and alkanes (C_{1-4}) were the main products from catalytic cracking of HDPE. It was also found that Y_G increased while Y_L and Y_C decreased with increasing Si/Al ratio of the catalysts. Besides, MZ-X achieved a higher liquid yield, but a lower gas yield than the corresponding HZ-X catalysts with same Si/Al ratio. Y_C on MZ-X were lower than on the corresponding HZ-X. The maximum Y_{TGP} (468 mL g^{-1}) and the highest $C_{2-4}^=$ selectivity (44%) were achieved over the HZ-150. The highest Y_L (21.5%) and BTEX selectivity (87.6%) were achieved over MZ-27.

Combing the analysis on acidity and pore structure of catalysts, we deduced that the amount of acidic sites was mainly responsible for the formation of liquid products and coke, while a mesoporous structure facilitated the formation of liquid products. Acidic active sites were necessary for improving the decomposition of polymers *via* carbonium ion and β-scission reaction mechanisms. Meanwhile, acidic active sites were also necessary for the formation of aromatic products *via* cyclization and dehydrogenation reaction of cracking fragments. However, the over-crowded acidic sites could cause excessive coupling reaction of aryl groups through a carbonium ion reaction mechanism, leading to the formation of cokes (*e.g.* HZ-27). Therefore, optimization and modification of the acidic property of zeolites are important to improve product selectivity. Addition of MCC in synthesis process of zeolites enhanced the formation of mesopores, and thus improved the mass transfer and diffusion rate of reactants and intermediate products, consequently restraining the secondary reactions *e.g.* coking and accelerating the formation of liquid products.[33] The presence of a substantial proportion of benzene, toluene and xylene in liquid product (Table 3), indicates that catalytic cracking of HDPE over MZ-27 is a potential technique to selectively produce BTEX *via* a non-petroleum route.

For the catalysts with high Si/Al ratio *e.g.* HZ-150 and MZ-150, the moderate acid sites on zeolites (Table 2) could be adequate for catalytic scission of polymers into micromolecule fragments, but inadequate for the formation of aromatics-rich liquid products *via* multi-position adsorption and activation of these micromolecule fragments.[34] Therefore, a lot of gas products were produced on these catalysts. The presence of more aliphatic hydrocarbons (16.9–19.2%) in HZ-150 and MZ-

Table 4 Product yield and product distribution from cracking of PP over the prepared catalysts

	Catalysts					
	HZ-27	MZ-27	HZ-80	MZ-80	HZ-150	MZ-150
Y_{TGP} (mL g^{-1})	353	331	367	348	412	381
Y_L (%)	29.3	32.1	24.1	27.2	22.8	25.3
Y_C (%)	1.2	1.0	0.8	0.6	0.5	0.2
Y_G (%)	69.5	66.9	75.1	72.2	76.7	74.5
Gas product (%)						
C_2H_4	15.0	12.8	15.5	14.3	15.1	13.1
C_3H_6	17.1	14.5	20.1	17.3	25.6	22.4
n-C_4H_8	4.9	4.5	6.3	5.4	7.6	9.1
CH_4	8.1	6.5	6.9	6.1	3.7	3.1
C_2H_6	5.9	4.7	5.4	5.9	3.5	4.6
C_3H_8	17.4	23.1	20.1	22.8	10.8	13.9
n-C_4H_{10}	4.5	3.8	4.6	4.6	3.4	4.0
$C_{2-4}^=$	37.0	31.8	41.9	37.0	48.3	44.6
C_{1-4}	35.9	38.1	37.0	39.4	21.4	25.6
Others	27.1	30.1	21.1	23.6	30.3	29.8
Liquid product (%)						
Benzene	7.5	8.1	6.2	7.9	5.3	4.8
Toluene	23.3	24.9	22.1	23.5	18	22.6
Ethylbenzene	5.4	5.6	5	5.1	5.1	4.9
Xylene	38.2	41.1	37.8	38.5	32.4	31.9
BTEX	74.4	79.7	71.1	75	60.8	64.2
Aliphatic hydrocarbons	12.2	11.5	17.8	15.8	30.7	30.3
Others	13.4	8.8	11.1	9.2	8.5	5.5

150 derived liquid products, indicates an incomplete aromatization reactions occurring on these catalysts.

If considering the importance of both light olefins and BTEX in industrial applications, HZ-150 and MZ-27 exhibited their own great application potential.

Artetxe et al. carried out a similar research on cracking HDPE on HZSM-5 with different Si/Al ratios in a thermal-catalytic two-step unit (spouted bed connected by fixed bed).[35] The maximum light olefin yield was 58 wt%, obtained at 500 °C using the most acidic catalyst (Si/Al = 30). This disagrees with our results. The maximum light olefin yield (37.6%) in our study was achieved over the weakest acidic catalyst (HZ-150). The smaller pore could inhibit polymer oligomers accessing the active sites inside the pore of zeolite; the high temperature (550 °C) could accelerate secondary reactions e.g. aromatization and coking; the fixed bed reactor used in our study could cause heat transfer limitation. These factors led to a lower light olefin yield in our study. Other studies on cracking plastics over HZSM-5 were found to be about selective production of light olefins. Plastics were commonly cracked in fluidized-bed or spouted bed reactors at a temperature of 400–500 °C. A gas yield of 60–88% with light olefins selectivity of 40–75% were achieved.[36,37] Besides,
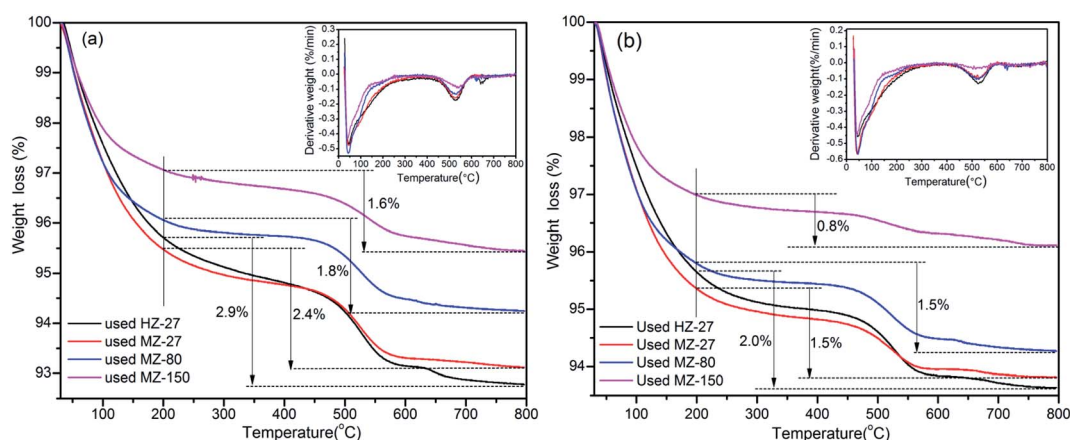

Fig. 6 TGA and DTG profiles of the used catalysts from cracking HDPE (a) and PP (b).

Table 5 Liquid product composition from cracking of HDPE and PP over HZ-27 and MZ-27[a]

No.	RT (min)	Compounds	Molecular formula	HZ-27 (HDPE)	MZ-27 (HDPE)	HZ-27 (PP)	MZ-27 (PP)
				Catalysts and feedstocks area (%)			
1	1.71	Cyclopentane, methyl-	C_6H_{12}	1.0	0.5	1.5	0.8
2	1.81	1,4-Pentadiene, 2-methyl-	C_6H_{10}	0.9	0.3	0.8	0.7
3	1.87	Benzene	C_6H_6	5.9	8.8	7.5	8.1
4	1.97	Cyclopentane, 1,3-dimethyl-, trans-	C_7H_{14}	0.5	—	0.5	0.4
5	2.04	Heptane	C_7H_{16}	0.5	0.3	0.6	—
6	2.17	Cyclopentene, 1,5-dimethyl-	C_7H_{12}	0.3	0.2	0.5	0.3
7	2.25	Cyclohexane, methyl-	C_7H_{14}	0.5	0.4	0.2	—
8	2.34	Cyclopentane, ethyl-	C_7H_{14}	0.4	—	0.1	0.1
9	2.40	Cyclohexene, 4-methyl-	C_7H_{12}	0.5	—	0.4	0.3
10	2.52	Cyclobutane, (1-methylethylidene)-	C_7H_{12}	1.0	0.5	0.8	0.8
11	2.64	Heptane, 4-methyl-	C_8H_{14}	—	—	—	0.9
12	2.70	Toluene	C_7H_8	23.4	28.3	23.4	24.9
13	3.05	Octane	C_8H_{18}	0.8	—	0.6	0.2
14	3.24	1,3-Dimethyl-1-cyclohexene	C_8H_{14}	0.4	—	1.2	1.3
15	3.41	Heptane, 2,4-dimethyl-	C_9H_{20}	—	—	0.5	0.5
16	3.63	Cyclohexane, 1,3,5-trimethyl-	C_9H_{18}	—	—	1.6	1.6
17	4.01	1,2,4,4-Tetramethylcyclopentene	C_9H_{16}	—	—	0.6	0.3
18	4.15	Cyclohexane, 1,3,5-trimethyl-, (1-alpha, 3-alpha, 5-beta)-	C_9H_{18}	—	—	2.0	2.3
19	4.31	Ethylbenzene	C_8H_{10}	7.4	5.7	5.4	5.6
20	4.57	p-Xylene	C_8H_{10}	36.3	36.6	31.5	32.8
21	5.18	o-Xylene	C_8H_{10}	5.1	8.3	6.8	8.4
22	5.30	Nonane	C_9H_{20}	0.5	0.3	—	—
23	6.85	Benzene, propyl-	C_9H_{12}	0.6	5.3	0.4	0.3
24	7.05	Benzene, 1-ethyl-3-methyl-	C_9H_{12}	6.9	0.2	2.8	1.2
25	7.51	Benzene, 1-ethyl-2-methyl-	C_9H_{12}	—	1.2	2.5	1.8
26	7.84	Benzene, 1,2,3-trimethyl-	C_9H_{12}	0.8	—	1.3	0.8
27	8.19	Nonane, 2,6-dimethyl-	$C_{11}H_{14}$	—	0.6	0.7	1.3
28	8.79	Indane	C_9H_{10}	0.6	0.3	0.6	0.4
29	9.14	Benzene, 1-methyl-3-propyl-	$C_{10}H_{14}$	0.5	—	0.5	0.4
30	9.22	Benzene, 1-methyl-4-propyl-	$C_{10}H_{14}$	0.8	—	0.6	0.3
31	9.76	Benzene, 1-methyl-2-(2-propenyl)-	$C_{10}H_{12}$	—	—	0.2	0.2
32	9.86	Benzene, 1-methyl-4-(2-propenyl)-	$C_{10}H_{12}$	—	—	0.2	0.4
33	10.08	Undecane	$C_{11}H_{24}$	0.3	0.4	—	—
34	10.87	1H-Indene, 2,3-dihydro-4-methyl-	$C_{10}H_{12}$	0.3	0.2	0.5	0.3
35	11.06	Benzene, 1-methyl-1,2-propadienyl-	$C_{10}H_{10}$	0.2	1	—	—
36	11.67	Naphthalene	$C_{10}H_8$	1.6	—	1.1	0.8
37	11.85	Dodecane	$C_{12}H_{26}$	0.6	—	—	—
38	12.44	Dodecane, 4,6-dimethyl-	$C_{14}H_{30}$	—	0.8	0.5	0.2
39	13.44	Naphthalene, 1-methyl-	$C_{11}H_{10}$	1.1	—	1.5	0.9
40	15.51	2,3-Dimethyldodecane	$C_{14}H_{30}$	—	—	0.5	0.2
41	15.87	Hexadecane, 3-methyl-	$C_{14}H_{30}$	—	—	0.5	0.1
42	17.29	Cetene	$C_{16}H_{32}$	0.4	—	—	—

[a] —: not detected.

the light aromatics selectivity in MZ-27 derived oil is 87.6%, which is similar to that reported in previous study, obtained from catalytic pyrolysis of industrial plastic waste on Ga-ZSM-5 (aromatic content >80%).[15] In order to improve light aromatics yield, an increase in residence time should be considered.

3.2.2 Catalytic cracking of PP. Table 4 shows the yield and product distribution from catalytic cracking of PP over the prepared catalysts. Similar to cracking of HDPE, the highest Y_{TGP} (412 mL g^{-1}) and S_{LO} (48.3%) were obtained over HZ-150, while the highest Y_L (32.1%) and BTEX selectivity (79.7%) were achieved over MZ-27. The Y_L from cracking of PP were much higher than that from cracking of HDPE over the same catalyst. This is probably attributed to the different chemical structures of PP and HDPE. Due to the existence of pendant methyl group, the bond dissociation energy of PP (334.4 kJ mol^{-1}) is lower than that of HDPE (341.1 kJ mol^{-1}), therefore, PP is active to generate cracking fragments.[38] In a limited time, the larger fragments could rapidly escape from reactor without undergoing further secondary reactions and directly become liquid products, while the smaller fragments (ethylene or propylene) could combine each other to form aromatic products via Diels–Alder reaction upon passing through the catalyst bed. More aliphatic hydrocarbons were present in PP-derived liquid oil, demonstrating that a weaker secondary reaction such as cyclization and aromatization occurred during cracking process.
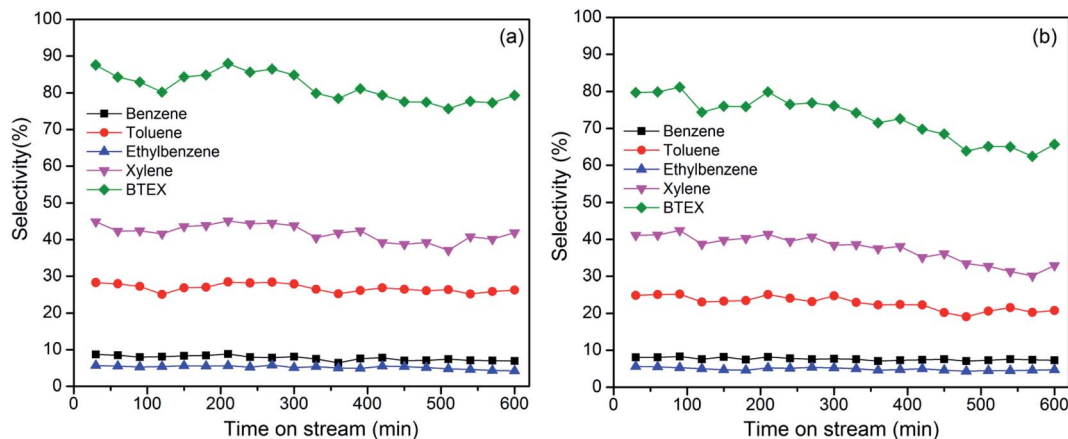
Fig. 7 BTEX selectivity with time on stream from cracking of HDPE (a) and PP (b) over MZ-27 at 550 °C.

It was found that regardless of PP and HDPE, propylene selectivity increased whereas C$_{1-4}$ selectivity decreased with increasing Si/Al ratio of catalysts. This would be ascribed to the acidity of catalysts. The dense acid sites present on HZ-27 and MZ-27 helped to improve cracking of polymers, and also subsequent secondary reactions of cracking fragments, consequently leading to formation of more stable gas (C$_{1-4}$) and liquid products (e.g. aromatics). The catalysts with high Si/Al ratio e.g. HZ-150 and MZ-150, had less acid sites, and thus a relatively weaker secondary reaction of cracking fragments could occur on its surfaces, therefore, more propylene was present in gas products. Isopentane, pentylene, isobutylene and butadiene were probably produced during the cracking process but could not be identified with the present standard gas. Accordingly, they were classified in other gas products.

3.2.3 Coke analysis. As can be seen in Tables 3 and 4, the coke yields from catalytic cracking of both polymers decreased with increasing Si/Al ratio of the catalysts, suggesting that the acid amount was mainly responsible for the formation of coke.[39] The highest Y_C from cracking of HDPE and PP were 1.6% and 1.2%, respectively, obtained over HZ-27. In addition, for both polymers the Y_C on the MZ-X were always lower than the corresponding HZ-X with the same Si/Al ratio, indicating that MZ-X had better anti-coking ability. The presence of more mesopores in MZ-X would account for its better anti-coking ability.[40]

The TGA and DTG profiles of the spent catalysts are shown in Fig. 6. The weight loss below 200 °C mainly resulted from the removal of physically adsorbed water, the weight loss between 200–500 °C could be attributed to the oxidation of light coke, while weight loss between 500–800 °C was probably due to the oxidation of heavy coke such as stable graphite.[41] The order of weight loss between 200–800 °C (coke amount) for different catalysts was: HZ-27 > MZ-27 > MZ-80 > MZ-150. The trend of coke amount from TGA agrees with the results obtained from calcination method. These results indicate that a mild acidity and a larger pore structure would be helpful for restraining the formation of coke and improving the lifetime of catalysts.

3.2.4 Liquid product analysis and catalytic reaction mechanism. Table 5 lists the composition of liquid products

yielded from catalytic cracking of HDPE and PP over HZ-27 and MZ-27. The major components of HDPE-derived liquid products were similar to those from PP. The liquid products mainly contained benzene (5.9–8.8%), toluene (23.4–28.3%), ethylbenzene (5.4–7.4%), p-xylene (31.5–36.6%), o-xylene (5.1–8.4%) and a considerable amount of cyclanes (1.4–6.7%) and cycloolefins (0.2–2.7%). The selectivity to p-xylene were higher than 30% for two type of polymers, indicating the wide application foreground of present catalysts for producing p-xylene which is a product heavily short of in our country.

Combined with the results of current reports,[40,42] the possible reaction pathway of HDPE and PP decomposition were concluded as follows. Catalytic cracking of polyolefins includes pyrolysis and catalytic cracking reactions. The polyolefin is firstly cracked into volatile alkyl radicals via random scission of the long chains of the polymers at high temperature according to free radical mechanism.[34] The volatile components subsequently undergo a series of further secondary reactions including cracking, Diels–Alder reaction, dehydrogenation, hydrogen transfer and aromatization upon passing through catalyst bed according to a carbenium ion mechanism, consequently leading to the formation of gas products e.g. ethylene and propylene, and liquid products including cyclic hydrocarbons (1,3-dimethyl-cyclopentane, methyl-cyclohexane, 1,5-dimethyl-cyclopentene, 4-methyl-cyclohexene) and aromatic products.[42] Compared to HDPE, more C9 hydrocarbons (propylene oligomer) present in PP-derived oil, which would result from breakage of PP chain at tertiary carbons.

3.3 Stability of the catalysts

Fig. 7 shows the results for the continuous cracking of HDPE and PP in 300 min. The collected liquid oil during 1 min ranged from 0.02–0.03 g for HDPE, and 0.03–0.04 g for PP. BTEX selectivity decreased from 87.6% to 79.3% for HDPE, and from 80% to 65.7% for PP after 300 min. Xylene and toluene selectivity decreased slightly with increasing reaction time. Carbon deposition on catalysts could result in the decrease in catalytic activity. The presence of the pendant methyl groups increases the effective cross-section of the PP oligomers, indicates that PP

molecules are more difficult to diffuse into the pore of the zeolite compared to HDPE. This inhibits the aromatization reaction of PP. The stability of the synthesized MZ-27 catalyst should be further improved in the successive research.[38]

4. Conclusions

ZSM-5 zeolites with micro–mesopore structure were successfully prepared by introducing MCC as co-template into hydrothermal synthesis process. The higher Si/Al ratio led to the formation of zeolites with less acid sites. MCC-adding ZSM-5 (MZ-X) exhibited higher mesopore volume and more strong acid sites compared to the MCC-free HZ-X zeolites. The resultant ZSM-5 were used for catalytic cracking of HDPE and PP. MZ-27 which possessed more acid sites and mesopores achieved the highest oil yields: 21.5% for HDPE and 32.1% for PP, and the BTEX selectivity therein were 87.6% and 79.7%, respectively. HZ-150 which possessed more micropores and less acid sites obtained the highest gas yields: 85.4% for HDPE and 76.7% for PP, and the $C_{2-4}^{=}$ selectivity therein were 44% and 48.3%, respectively. It was concluded that the acidity and porous structure of catalysts significantly affected the conversion and product distribution. MCC as an economical and renewable resource showed potential application prospects to be used as template to modulate pore structure and acidity of zeolites.

Conflicts of interest

Authors declare no competing interest.

Acknowledgements

Notes and references

1 C. D. Zhang, G. Kwaket, Y. J. Lee, K. W. Jun, R. X. Gao, H. G. Park, S. Kim, J. E. Min, S. C. Kang and G. F. Guan, Microporous Mesoporous Mater., 2019, 284, 316–326.

2 R. Geyer, J. R. Jambeck and K. L. Law, Sci. Adv., 2017, 3, e1700782.

3 S. D. A. Sharuddin, F. Abnisa, W. A. M. W. Daud and M. K. Aroua, Energy Convers. Manage., 2016, 115, 308–326.

4 A. K. Panda, R. K. Singh and D. K. Mishra, Renewable Sustainable Energy Rev., 2010, 14, 233–248.

5 J. R. Jambeck, R. Geyer, C. Wilcox, T. R. Siegler, M. Perryman, A. Andrady, R. Narayan and K. L. Law, Science, 2015, 347, 768–771.

6 G. H. Song, H. Zhang, H. B. Duan and M. Xu, Resour., Conserv. Recycl., 2018, 130, 226–227.

7 H. A. Arafat, K. Jijakli and A. Ahsan, J. Cleaner Prod., 2015, 105, 233–240.

8 W. K. Kamal and P. Vijayabalan, Waste Manag., 2016, 51, 91–96.

9 D. P. Serrano, J. Aguado, J. M. Escola, E. Garagorri, J. M. Rodrgueza, L. Morselli, G. Palazzi and R. Orsic, Appl. Catal., B, 2004, 49, 257–265.

10 G. Lopez, M. Artetxe, M. Amutio, J. Bilbao and M. Olazar, Renewable Sustainable Energy Rev., 2017, 73, 346–368.

11 R. Miandad, M. A. Barakat, A. S. Aburiazaiza, M. Rehan and A. S. Nizami, Process Saf. Environ. Prot., 2016, 102, 822–838.

12 B. Kunwar, H. N. Cheng, S. R. Chandrashekaran and B. K. Sharma, Renewable Sustainable Energy Rev., 2016, 54, 421–428.

13 K. Akubo, M. A. Nahil and P. T. Williams, J. Energy Inst., 2019, 92, 195–202.

14 J. Nishino, M. Itoh, H. Fujiyoshi and Y. Uemichi, Fuel, 2008, 87, 3681–3686.

15 J. Aguado, J. L. Sotelo, D. P. Serrano, J. A. Calles and J. M. Escola, Energy Fuels, 1997, 11, 1225–1231.

16 Z. H. Zhang, H. Cheng, H. Chen, K. Q. Chen, X. Y. Lu, P. K. Ouyang and J. Fu, Bioresour. Technol., 2018, 256, 241–246.

17 D. P. Gamliel, H. J. Cho, W. Fan and J. A. Valla, Appl. Catal., A, 2016, 522, 109–119.

18 H. Chen, X. Shi, J. F. Liu, K. C. Jie, Z. H. Zhang, X. B. Hu, Y. M. Zhu, X. Y. Lu, J. Fu, H. Huang and S. Dai, J. Mater. Chem. A, 2018, 6, 21178–21185.

19 Q. Y. Wang, S. T. Xu, J. R. Chen, Y. X. Wei, J. Z. Li, D. Fan, Z. X. Yu, Y. Qi, Y. L. He, S. L. Xu, C. Y. Yuan, Y. Zhou, J. B. Wang, M. Z. Zhang, B. L. Su and Z. M. Liu, RSC Adv., 2014, 4, 21479–21491.

20 Q. Zhang, S. Hu, L. L. Zhang, Z. J. Wu, Y. J. Gong and T. Dou, Green Chem., 2013, 1, 77–81.

21 S. Vichaphund, D. Aht-ong, V. Sricharoenchaikul and D. Atong, Renewable Energy, 2015, 79, 28–37.

22 X. Li, C. Gu and B. Zhong, J. Mol. Catal., 1992, 6, 104–112.

23 K. Niemelä and E. Sjöström, Biomass, 1986, 11, 215–221.

24 B. Y. Yang and R. Montgomery, Carbohydr. Res., 1996, 280, 27–45.

25 G. Nazeri, S. B. Liaw, Y. Yu and H. W. Wu, Fuel, 2018, 218, 174–178.

26 Y. Sang, Q. Z. Jiao, H. S. Li, Q. Wu, Y. Zhao and K. N. Sun, J. Nanopart. Res., 2014, 16, 2755.

27 D. P. Serrano, J. Aguado, J. M. Escola, J. M. Rodriguez and A. Peral, J. Catal., 2010, 276, 152–160.

28 C. Engtrakul, C. Mukarakate, A. K. Starace, K. A. Magrini, A. K. Rogers and M. M. Yung, Catal. Today, 2016, 269, 175–181.

29 L. Rodríguez-González, F. Hermes, M. Bertmer, E. Rodríguez-Castellón, A. Jiménez-López and U. Simon, Appl. Catal., A, 2007, 328, 174–182.

30 S. Sang, F. Chang, Z. Liu, C. He, Y. He and L. Xu, Catal. Today, 2004, 93–95, 729–734.

31 C. Y. Liu, W. Y. Gu, D. J. Kong and H. C. Guo, Microporous Mesoporous Mater., 2014, 183, 30–36.

32 N. Y. Kang, B. S. Song, C. W. Lee, W. C. Choi, K. B. Yoon and Y. K. Park, Microporous Mesoporous Mater., 2009, 118, 361–372.

33 Y. H. Kim, K. H. Lee, C. M. Nam and J. S. Lee, ChemCatChem, 2012, 4, 1143–1153.

34 K. Sun, Q. X. Huang, Y. Chi and J. H. Yan, *Waste Manag.*, 2018, **81**, 128–137.

35 M. Artetxe, G. Lopez, M. Amutio, G. Elordi, J. Bilbao and M. Olazar, *Ind. Eng. Chem. Res.*, 2013, **52**, 10637–10645.

36 M. D. R. Hernandez, A. N. Garcia, A. Gomez, J. Agullo and A. Marcilla, *Ind. Eng. Chem. Res.*, 2006, **45**, 8770–8778.

37 J. F. Mastral, C. Berrueco, M. Gea and J. Ceamanos, *Polym. Degrad. Stab.*, 2006, **91**, 3330–3338.

38 Q. Zhou, L. Zheng, Y. Z. Wang, G. M. Zhao and B. Wang, *Polym. Degrad. Stab.*, 2004, **84**, 493–497.

39 G. Elordi, M. Olazar, M. Artetxe, P. Castano and J. Bilbao, *Appl. Catal., A*, 2012, **415–416**, 89–95.

40 Y. M. Ni, A. M. Sun, X. L. Wu, G. L. Hai, J. L. Hu, T. Li and G. X. Li, *J. Colloid Interface Sci.*, 2011, **361**, 521–526.

41 P. Castaño, G. Elordi, M. Olazar, A. T. Aguayo, B. Pawelec and J. Bilbaoa, *Appl. Catal., B*, 2011, **104**, 91–100.

42 K. Sun, Q. Huang, M. Ali, Y. Chi and J. Yan, *Energy Fuels*, 2018, **32**, 5471–5479.